A combined in situ AFM and SEM study of the interaction between celestite (0 0 1) surfaces and carbonate-bearing aqueous solutions

Nuria Sánchez-Pastor, Carlos M. Pina *, Lurdes Fernández-Díaz

Departamento de Cristalografía y Mineralogía, Universidad Complutense de Madrid, 28040 Madrid, Spain

Abstract

In this paper, we present in situ atomic force microscopy (AFM) observations of the interaction between celestite ($SrSO_4$) (0 0 1) surfaces and Na_2CO_3 aqueous solutions. The observations indicate that the interaction is characterized by a rapid alteration (carbonatation) and dissolution of the original surface, shortly followed by the formation of a new phase. EDX analyses indicate that the new phase is strontianite ($SrCO_3$). Its crystallization involves the formation and spreading of islands of about 2.75 nm in height, which chiefly occurs on the step edges of the dissolving celestite substrate. The thickness of the islands remains almost constant during their spreading, which occurs mainly parallel to the celestite [0 1 0] direction. As a result of the progressive coalescence of the islands, a fairly homogeneous epitaxial layer forms on the celestite (0 0 1) face. At the initial stages, the formation of islands on the celestite (0 0 1) faces enhances dissolution, indicating the existence of a coupling between dissolution and crystallization reactions. Our measurements on series of AFM images provided quantitative information about coupled dissolution-growth rates on a nanoscale. The effect of the coupled reactions on the celestite (0 0 1) surface on a microscopic scale was also studied by scanning electron microscopy (SEM).

Keywords: Dissolution–crystallization; Celestite; Strontianite; Atomic force microscopy; Scanning electron microscopy

1. Introduction

Celestite ($SrSO_4$) is a relatively common sulphate in the Earth's Crust, where it frequently occurs in association with gypsum, dolomite, calcite and halite [1]. In addition, celestite forms a solid solution with barite ($BaSO_4$). In nature, this solid solution shows a marked chemical bimodality, i.e. only Ba-rich or Sr-rich terms of the $Ba_xSr_{1-x}SO_4$ solid solution are frequent [2]. The thermodynamic character of the $Ba_xSr_{1-x}SO_4$ solid solution has been largely disputed, although most recent works consider it nearly ideal and, consequently, almost complete at 25 °C. Therefore, its chemical bimodality cannot be completely justified on the basis of thermodynamics [3 and references therein]. Moreover, even considering this solid solution as ideal, the large difference between the solubility products of its end-members (the solubility product for barite at 25 °C is $K_{sp,barite} = 10^{-9.98}$ [4], while for celestite is $K_{sp,celestite} = 10^{-6.63}$ [5]) determines that the geochemical conditions that would allow to precipitate intermediate solid solutions are very restrictive. Thus, the chemical bimodality of this solid solution can be considered a consequence of the important differences in crystallization kinetics resulting from the high difference in solubility between the two end-members [6,7].

It has also been pointed out that crystals of celestite–barite solid solution could act as precursors for the formation of other phases relatively common in nature, mainly carbonates corresponding to the $Ba_xSr_{1-x}CO_3$ solid solution [8]. The fact that intermediate compositions of $Ba_xSr_{1-x}CO_3$ solid solution are, as it occurs in the case of the $Ba_xSr_{1-x}SO_4$ solid solution, rare in nature, together with a difference between the ionic radii of Sr^{2+} (1.31 Å) and Ba^{2+} (1.47 Å) of 10.88%, supported the idea of the existence of a miscibility gap at low temperatures [8].

* Corresponding author. Tel.: +34 91 3944879; fax: +34 91 3944872.
E-mail address: cmpina@geo.ucm.es (C.M. Pina).

promotes further celestite dissolution. As a result, while the concentration of carbonate in the solution is maintained high enough, the release of Sr^{2+} guarantees the growth of strontianite islands. The depletion of carbonate in the solution and the increase of the thickness of the carbonate layer, which progressively armours the celestite (001) surface from further interaction with the aqueous solution, should determine a progressive slowing down of the dissolution–crystallization process. In addition, the growth of $SrCO_3$ has a secondary effect: the increase of the SO_4^{2-}/CO_3^{2-} ratio in the surrounding aqueous solution. As this ratio increases, the celestite dissolution rate decreases because a lesser amount of Sr^{2+} is required to reach saturation with respect to celestite. Although most of the celestite (001) surface becomes covered by the strontianite layer, the celestite dissolution and the strontianite growth coupled processes can continue to progress in crevices originated during the cleavage. In those areas, strontianite grows as aggregates with very rough surfaces, indicating that, locally, the supersaturation with respect to strontianite is very high (see Fig. 7a and b). In the system under consideration a true-equilibrium is not reached since the initial solid (celestite) becomes progressively isolated from the aqueous solution by a coating layer of a secondary solid (strontianite). Therefore, we can assume that the system approaches a state usually referred to as "partial equilibrium" [26,27].

Regardless of the development of the dissolution–crystallization process at a local scale, our experimental results demonstrate that the celestite dissolution and strontianite growth reactions are coupled. Furthermore, there is positive feedback between both reactions. The behaviour observed is similar to that described by Pina et al. [28] for the case of the solvent-mediated transformation of phosgenite into cerussite. AFM observations carried-out by these authors showed a significant enhancement of the dissolution rate of phosgenite once cerussite nucleated on its surface, concluding that, at some stage in the enhancement process, a balance would be achieved between the rate of dissolution and the rate of precipitation. In the case of the celestite–strontianite system, we can also conclude that determining overall reaction rates for processes which involve simultaneous dissolution and crystallization reactions must be done taking into account both the spatial and temporal relationships between these reactions on a molecular scale.

6. Concluding remarks

1. The presence of Na_2CO_3 in the aqueous solution modifies the dissolution behaviour of the celestite (001) surface. The most remarkable feature is the enhancement of the dissolution rate, which increases with the initial concentration of Na_2CO_3 in the aqueous solution. Moreover, the etch pits modified their shape in comparison to that shown when dissolution occurs in deionised water. Thus, the etch pits lose their characteristic straight edges and become elliptical. Another interesting feature is the initial alteration of the celestite (001) surface, which seems to occur prior to the formation of the etch pits and probably as a result of the carbonatation of this surface.
2. AFM observations show that the formation of islands of a new phase shortly occurs after the beginning of the alteration and dissolution of the original surface. The islands of the new phase show an almost constant thickness ($\sim 2.75 \pm 0.25$ nm) during their spreading on the celestite (001) surface. Nevertheless, on top of the surface of the islands, monolayers (2.9 ± 0.2 Å in height) that advance at a reduced rate continue to form simultaneously to the lateral growth of the islands.
3. SEM images of celestite surfaces after their interaction with carbonate solutions in the fluid cell show that crystal aggregates have formed in crevices. According to the results of the EDX analyses, the composition of those aggregates corresponds to that of strontianite ($SrCO_3$).
4. The height of the uppermost monolayers on the islands is in agreement with a half of the *c* lattice parameter in the strontianite structure (3.03 Å), i.e. the elementary growth layer for strontianite (001) faces. This suggests the existence of an epitaxy between the islands and the celestite substrate. The most probable epitaxial relations on the common (001) plane are: $[010]_{strontianite}//[100]_{celestite}$, and $[100]_{strontianite}//[010]_{celestite}$.
5. Dissolution rates on the celestite (001) substrate substantially increase once strontianite islands start to grow, indicating the existence of a coupling between dissolution and growth reactions. Such a coupling seems to control the kinetics of the solvent-mediated transformation of celestite into strontianite, indicating that celestite crystals can be replaced by strontianite as a result of interaction with carbonate aqueous solutions under room conditions.

Acknowledgements

N. Sánchez-Pastor acknowledges financial support from Spanish Ministry of Education and Science (FPI grant). This work has been financially supported by Spanish Ministry of Education and Science (Project CGL2004-02501) and Comunidad de Madrid (Project 910148). The authors thank the Centro de Microscopia (UCM) for kindly providing them access to the AFM. The manuscript has benefited from constructive criticisms by three anonymous reviewers.

References

[1] J.S. Hanor, Rev. Min. Geochem. 40 (2000) 193.
[2] J.S. Hanor, Am. Miner. 53 (1968) 1215.
[3] U. Becker, A. Fernández-González, M. Prieto, R. Harrison, A. Putnis, Phys. Chem. Miner. 27 (2000) 291.
[4] C.W. Blount, Am. Miner. 62 (1977) 942.
[5] E.J. Reardon, D.K. Armstrong, Geochim. Cosmochim. Acta 51 (1987) 63.

the ionic strength of the aqueous solution when high Na_2CO_3 concentrations are used. Calculations carried-out using PHREEQC show that a solution initially saturated with respect to celestite becomes highly undersaturated when Na_2CO_3 is added. In addition to the effect of Na_2CO_3 concentration on the activity of Sr^{2+} and SO_4^{2-} species in solution, the contribution of the effect of the alteration (carbonatation) of the celestite (001) face (resulting in the formation of a rough, labile and possibly amorphous monolayer) has to be considered. It seems that both effects efficiently enhance the dissolution of the celestite (001) face, when it occurs in contact with carbonate waters.

5.2. *Composition and growth of the new phase*

SEM images of celestite crystals removed from the AFM fluid cell after reacting with Na_2CO_3 solutions show celestite (001) faces partially replaced by dendritic crystals and lenticular aggregates. These crystals are spatially related to micrometric etch pits, crevasses and cleavage planes on celestite surfaces, originating a characteristic porous texture. A similar texture was observed after the partial conversion of celestite crystals by hydrothermal treatment in Na_2CO_3 and K_2CO_3 solutions [14]. In addition, EDX analyses of crystal aggregates show that they are composed of carbon and strontium exclusively. Therefore, both the morphology and texture of the crystals and the EDX analyses indicate that the crystals newly-formed on celestite are strontianite. This is further supported by the relatively frequent observation of crystal aggregates with pseudohexagonal symmetry, which can be interpreted as resulting from aragonite-type twining.

The formation of strontianite from celestite at low temperature can be explained by considering that, in the presence of carbonate solutions, the dissolution of celestite is enhanced. As a result of the dissolution process, Sr^{2+} and SO_4^{2-} ions are rapidly released to the solution. This leads to a progressive increase in supersaturation with respect to strontianite. Once a threshold value of supersaturation with respect to strontianite is overcome, nucleation of this phase occurs on the celestite (001) face. Therefore, the formation and spreading of nanometric islands correspond to the earliest stages of strontianite formation on celestite (001) surfaces. As AFM measurements show, strontianite islands rapidly reach a height of 2.75 ± 0.25 nm, which remains essentially constant until the coalescence of islands and leads to the formation of a more or less uniform strontianite layer on the celestite (001) surface. Layers with similar thickness (~3 nm) have also been observed to form on calcite $(10\bar{1}4)$ surfaces when, as a result of their interaction with some metal-bearing solutions, a dissolution–precipitation process occurs [17–19]. Both the formation of islands with similar heights on different surfaces and as a result of the interaction with different aqueous solutions suggests that the height of the islands is somehow controlled by the match between the structures and their elastic properties.

The case we are dealing with can be considered a heteroepitaxy in which the (001) planes of both celestite and strontianite seems to be parallel. Since the elementary growth layer of strontianite (001) faces is a half of the strontianite c_0 lattice parameter, i.e. 3.016 Å [20], the observation of a monolayer 2.9 ± 0.2 Å in height on the top of the thick strontianite layer (~2.75 ± 0.25 nm) supports the existence of such a parallelism. Therefore, the typical islands (as well as the uniform layer) on the celestite (001) face consist of approximately 9 strontianite d_{002} elementary growth layers. We have not found further evidence of parallelisms between the strontianite layer and the celestite substrate. However, on the basis of the similarity of lattice parameters, the most probable epitaxial relationships on the (001) plane are $b_{strontianite}//a_{celestite}$, and $a_{strontianite}//b_{celestite}$, i.e. the parallelism between the [100] and [010] directions. Strontianite is orthorhombic, space group *Pmcn*, with $a_0 = 5.106$ Å, $b_0 = 8.421$ Å and $c_0 = 6.031$ Å [21]. Celestite is also orthorhombic, space group *Pnma*, with $a_0 = 8.389$ Å, $b_0 = 5.365$ Å and $c_0 = 6.885$ Å [22]. From these lattice parameter data, calculated misfits through strontianite–celestite interface are: $[(b_{strontianite}-a_{celestite})/a_{celestite}] \times 100 = 0.38\%$ and $[(b_{celestite}-a_{strontianite})/a_{strontianite}] \times 100 = 5.07\%$. These quite low misfits suggest a good matching between both lattices through the interface. However, AFM observations show that the lateral spreading of the strontianite islands on the celestite (001) face is initially slower than their growth along the vertical direction. Therefore, the difference between celestite and strontianite structures must be high enough to hinder the advancement of strontianite islands on the celestite (001) surface. In contrast, the advance in height seems to be energetically more favourable and it occurs by means of the repeated strontianite nucleation. In addition, the profiles of the islands show a very sharp boundary between the substrate and the islands and no development of a wetting layer is observed. All these features correspond to a Volmer–Weber epitaxial growth mechanism, which is characterized by a low adhesion between the substrate and the overgrowth [23]. A deeper study of the strontianite–celestite epitaxy would require the development of a model based on the elastic properties of both phases, which is beyond the scope of this work.

5.3. *Coupling between dissolution and crystallization*

As was previously mentioned, AFM experiments were carried-out under static conditions and, therefore, the system was allowed to evolve towards equilibrium. In the absence of carbonate, dissolution would progress until the aqueous solution eventually reached saturation with respect to celestite. However, in the presence of carbonate, the supersaturation threshold [24,25] for the formation of strontianite nuclei is overcome before this occurs. The subsequent growth of strontianite islands on the celestite (001) face leads to a Sr^{2+} depletion in the solution, which in turn

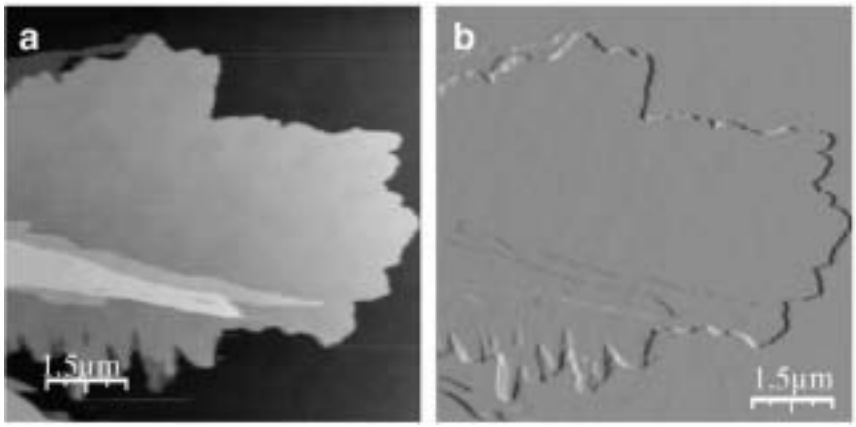

Fig. 8. (a) Height and (b) deflection AFM images of a newly-grown layer on the celestite (001) face after more than 2 h of exposure to a solution with an initial carbonate concentration of $[Na_2CO_3] = 0.002$ mol/l.

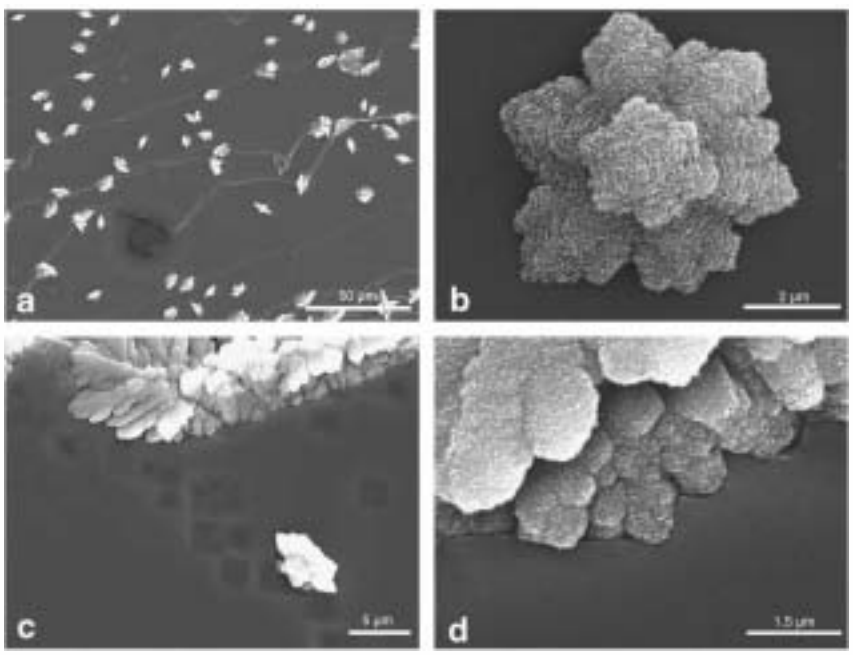

Fig. 9. SEM images of a celestite (001) face after exposure to a solution with a carbonate concentration of $[Na_2CO_3] = 0.1$ mol/l. (a) Newly-formed crystals, mainly located along partially dissolved celestite macrosteps. (b) Detail of a crystal aggregate with pseudohexagonal symmetry. (c) Boundary between newly-formed crystals and the dissolved celestite surface. (d) Detail of (c) showing the dissolution crystallization front.

the symmetry of the etch pits approaches the point symmetry of the unaltered celestite (001) face underneath, i.e. a two-fold axis, disappearing the 2_1 screw axis that relates triangular etch pits on the celestite (001) face. The morphological change of celestite etch pits from triangular to elliptical is similar to that observed by Risthaus et al. [16]. These authors have shown that background electrolytes (e.g. NaCl) are able to modify the shape of etch pits by ionic absorption on steps on celestite (001) faces. According to these authors Na^+ and Cl^- would increase the stability of steps parallel to the [010] direction compared to those steps parallel to the $\langle 120 \rangle$ directions. This explains the observed elongation of the etch pits shape along the [010] direction on the celestite (001) face when it dissolves in highly concentrated NaCl aqueous solutions. Na_2CO_3 has an effect on celestite step edges similar to that of NaCl. However, Na_2CO_3 is more effective in accelerating dissolution than NaCl, since similar dissolution rates along the celestite [010] and [100] directions are achieved for solutions with Na_2CO_3 concentrations about 300 times lower than the NaCl concentrations used by Risthaus et al. [16] in their dissolution experiments. To some extent, the enhancing of dissolution rates along [010] and [100] directions can be related to the decrease in the activity of Sr^{2+} and SO_4^{2-} ions when the aqueous solution contains Na_2CO_3. This is a direct consequence of the increase in

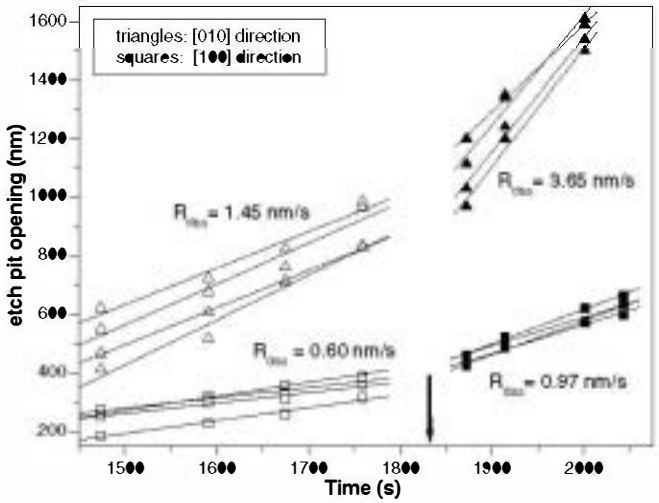

Fig. 6. Opening of the etch pits measured along the [010] (triangles) and [100] directions (squares) as a function of time. Open and black symbols indicate the etch pit growth before and after the nucleation of islands, respectively (the black arrow shows the time at which nucleation occurred). Note the change in the slopes (average dissolution rates, R_{diss}) once nucleation of the new phase on the dissolving surface occurred. The composition of the solution used in this experiment was $[Na_2CO_3] = 0.001$ mol/l.

[010] directions [15,16]. Our measurements on monolayer etch pits provided average dissolution rates of 0.25 ± 0.08 nm/s along the [100] direction and 1.06 ± 0.15 nm/s along the [010] direction. These values are in good agreement with celestite dissolution rates previously reported by Risthaus et al. [16]. According to these authors the dissolution rates of a celestite (001) surface in deionised water are around 1.03 ± 0.05 nm/s along the [010] direction and 0.28 ± 0.05 nm/s along the [100]. The high reproducibility of dissolution rate measurements on the celestite (001) face in deionised water gives a useful reference values to quantify the effect of both the presence of CO_3^{2-} ions in the solution and the formation and growth of a new phase on celestite dissolution behaviour.

Our AFM observations show that in the presence of carbonate, the dissolution behaviour of the celestite (001) face is strongly modified compared with deionised water. When there is carbonate in the solution, three main new features can be distinguished: (i) the alteration of celestite surfaces, (ii) the change in the etch pits shape from triangular to elliptical and (iii) the overall increase in dissolution rates.

Alteration of the celestite (001) surface is detected by an increase of its roughness, which can be related to the weakening and breaking of Sr–SO_4 outermost bonds in celestite by attachment of CO_3^{2-} ions on surface sites. The fact that surface roughness develops more rapidly as the carbonate concentration in the solution is higher is consistent with a progressive covering (and attack) of celestite (001) surfaces by CO_3^{2-}. This process can be considered a carbonatation of the celestite (001) surfaces on a molecular scale. As a consequence, the first celestite monolayers are somehow amorphised, favouring their subsequent removal. This is in agreement with the higher roughening of the surface around the etch pits. In addition, the elliptical shape developed by these etch pits during growth would indicate a lower crystallographic control of the dissolution compared to that observed when typical celestite triangular etch pits form in contact with deionised water. If we assume that the dissolving layers have been previously amorphised,

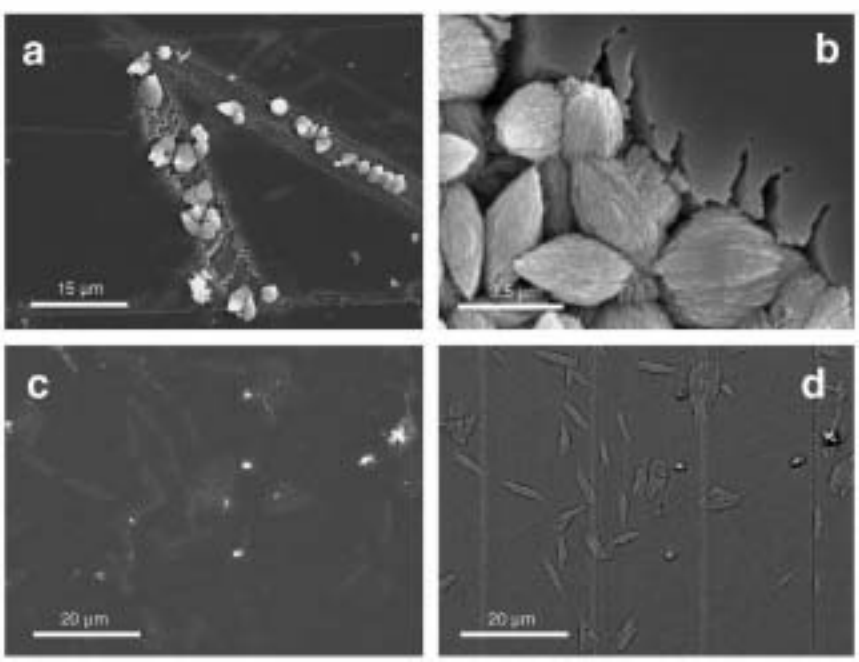

Fig. 7. SEM images of a celestite (001) face after exposure to a solution with a carbonate concentration of $[Na_2CO_3] = 0.002$ mol/l. (a) and (b) images show crystal aggregates of strontianite grown along celestite crevasses on the celestite surface. (c) Distribution of strontianite crystals on the celestite surface. (d) BSE image of (c) evidencing the different composition of newly-formed crystals and the celestite substrate.

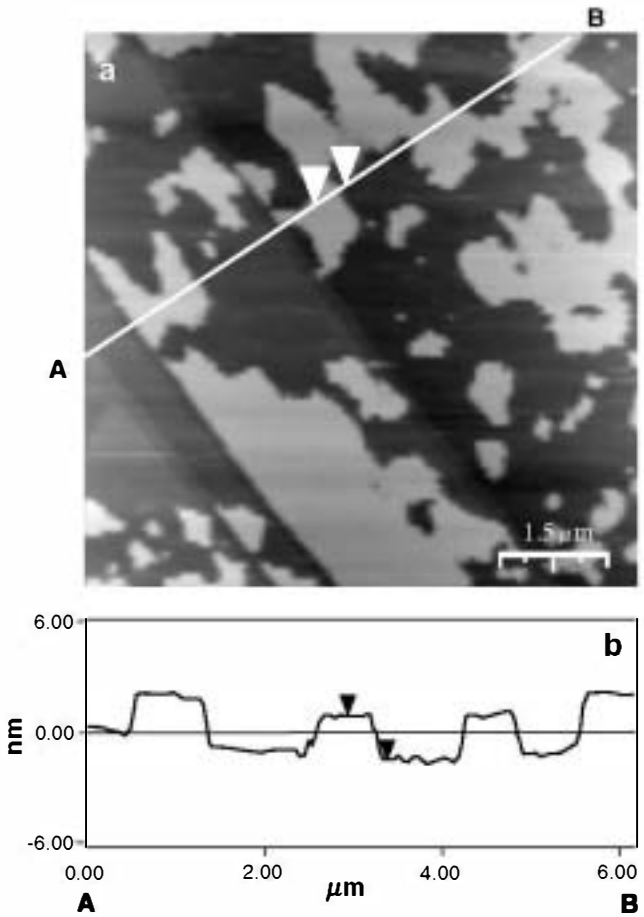

Fig. 3. (a) Height AFM image showing the layer of a new phase that partially covers the original celestite (001) surface. (b) Height profile along line A B. The vertical distance between the triangular indicators on (a) is 2.52 nm. The composition of the used solution was $[Na_2CO_3] = 0.002$ mol/l.

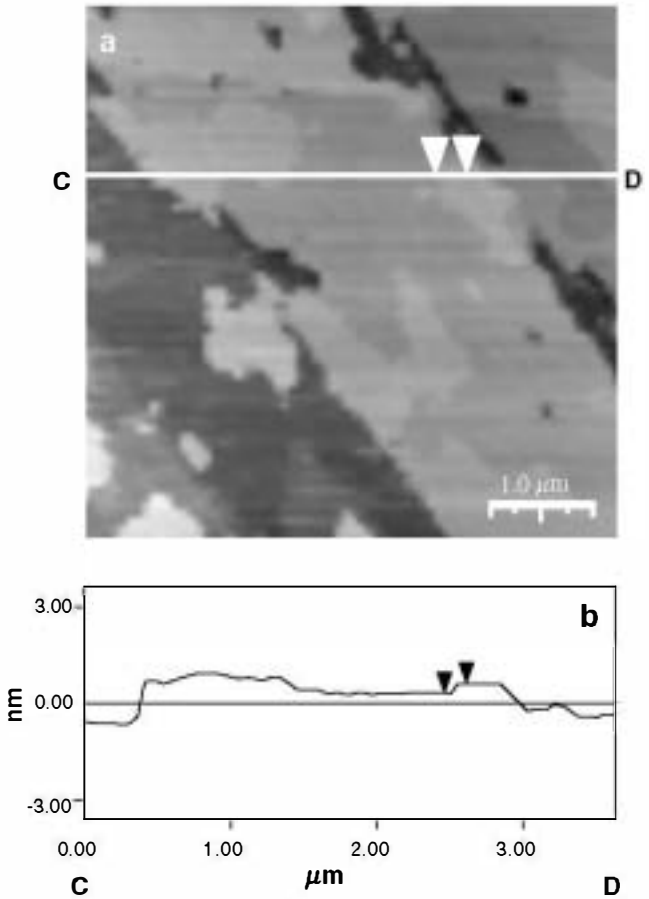

Fig. 4. (a) Height AFM image showing the growth of a monolayer over the thick layer (2.52 nm in height). (b) Height profile along the line C D. The vertical distance between the triangular indicators on (a) is 2.9 Å. The composition of the used solution was $[Na_2CO_3] = 0.002$ mol/l.

The newly-formed crystals were also analyzed by EDX. Only peaks corresponding to strontium and carbon were detected, but none corresponding to sulphur. This is consistent with a composition of $SrCO_3$ for the crystals.

Finally, when carbonate solutions with concentration $[Na_2CO_3] = 0.1$ mol/l were used, the growth and coalescence of islands leads to the development of large crystals on the celestite (001) surfaces. Fig. 9 shows crystals aggregates associated with partially dissolved celestite macrosteps and etch pits. In many cases, crystals adapt their shape to irregular dissolution fronts (Fig. 9c and d). These features clearly indicate that dissolution and growth processes occur simultaneously.

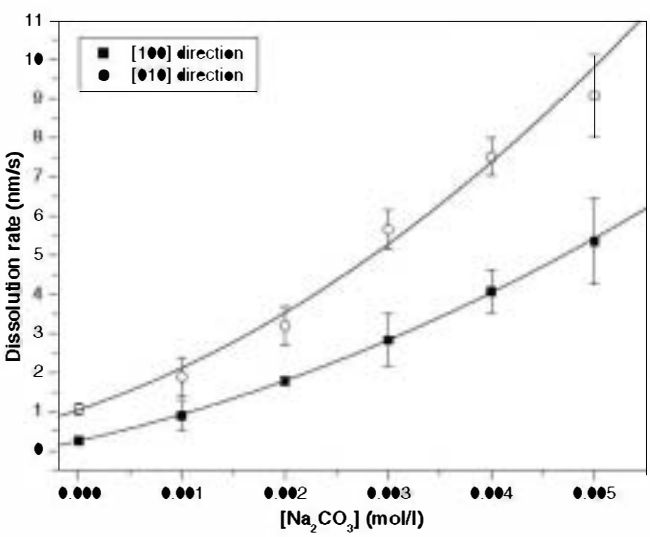

Fig. 5. Dissolution rates of the etch pits on the celestite (001) surface versus the total carbonate concentration in the aqueous solution. Dissolution rates were measured along the [010] and [100] directions. Standard deviation error bars have also been plotted. Data fit well to quadratic functions.

5. Discussion

5.1. Alteration/dissolution of celestite (001) surfaces in contact with carbonate aqueous solutions

In pure water, etch pits rapidly nucleate and grow on celestite (001) faces. These etch pits are one unit cell in depth (3.4 Å) and they show a characteristic triangular shape defined by step edges parallel to the ⟨120⟩ and

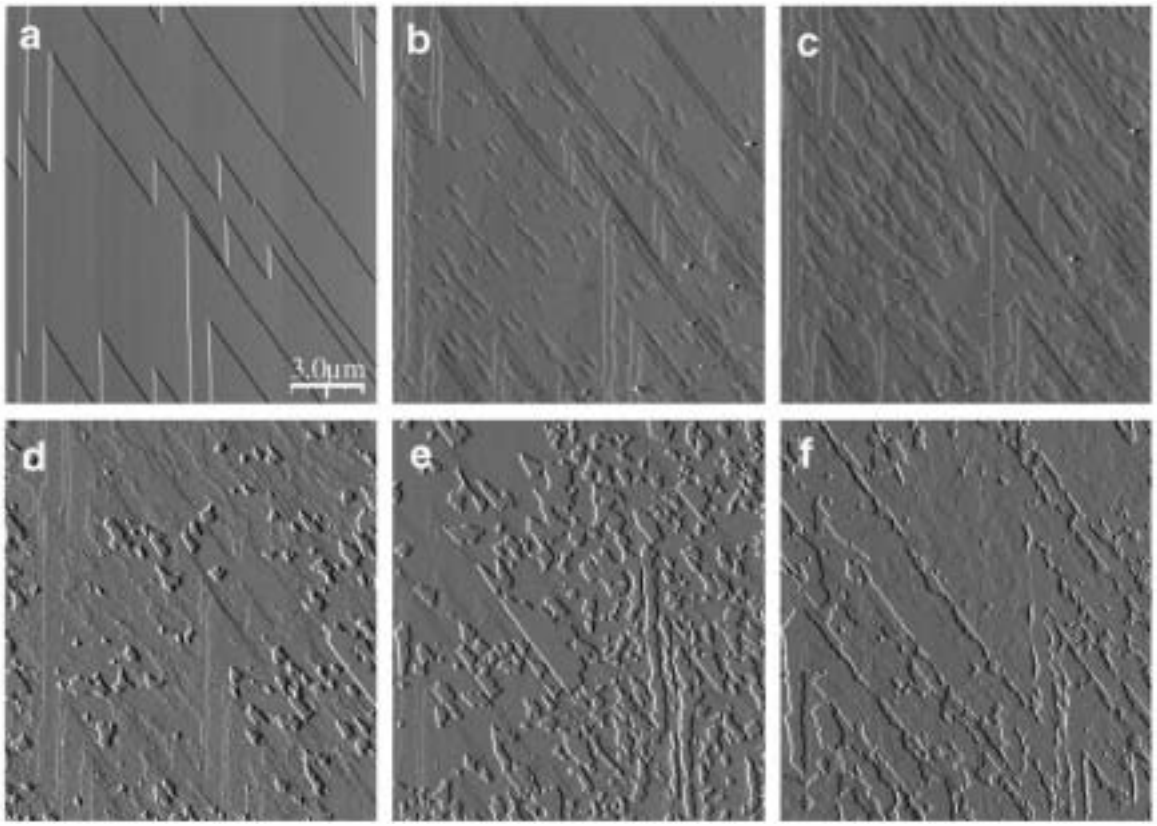

Fig. 2. Sequence of AFM deflection images showing (a–c) the dissolution of the celestite (001) surface and (d–f) the subsequent nucleation and spread of islands (~2.75 nm in height). In this case, the time elapsed between the beginning of the surface dissolution and the formation of the first island was approximately 20 min. The coalescence of islands leads to the formation of a fairly homogeneous layer ~35 min after starting the experiment. The composition of the used solution was $[Na_2CO_3] = 0.004$ mol/l.

the increase in size of the same etch pits after the formation of islands in their surroundings. From the slopes of the lines fitted to the experimental data, the average dissolution rates along the [100] and [010] directions before islands form are 0.60 nm/s and 1.45 nm/s, respectively. In contrast, calculated average dissolution rates after the nucleation of islands are 0.97 nm/s along the [100] direction and 3.65 nm/s along the [010]. These values represent an increase in the dissolution rates of around 50% and 140% along the [100] and [010] directions, respectively.

4. SEM observations and EDX analysis

The experiments were considered to be over when neither the dissolution of the substrate nor the growth of the islands were observed for periods longer than 30 min. Then, celestite crystals were recovered from the fluid cell and observed by SEM. In addition, the surfaces of the crystals were analyzed by EDX. SEM observations on the celestite (001) surface show the existence of a relationship between the initial carbonate concentration of the aqueous solutions and the degree of reaction (dissolution/crystallization) undergone by such surface. Thus, when a carbonate concentration of $[Na_2CO_3] = 0.001$ mol/l is used, neither newly-grown crystals nor etch pits could be detected on SEM images of the celestite (001) surface. However, when aqueous solutions with higher carbonate concentrations ($[Na_2CO_3] = 0.002$ mol/l) are used, large crystals corresponding to a new phase are clearly visible on the celestite (001) surface. These crystals form mainly on crevices of the original surface and on cleavage steps, as can be seen in Fig. 7a and b. In SEM images shown in Fig. 7c and d the distribution of crystals of the new phase on the celestite (001) surface can be clearly observed. Fig. 7d corresponds to the same area as Fig. 7c, but has been taken using backscattered electrons. The difference in brightness between the celestite surface and the newly-formed crystals results from a difference in composition. However, it is significant that the difference in brightness is not very marked. This can be related to the fact that the crystals shown in Fig. 7c and d are surrounded by the nanometric homogeneous layer previously observed by AFM. The similarity between the composition of such layer and the isolated crystals reduces the brightness contrast. When celestite (001) surfaces are in contact with a carbonate solution for longer than 2 h, the boundaries of the newly-formed layers observed in AFM images are dendritic, showing a very similar aspect to those observed on the SEM images (Fig. 8).

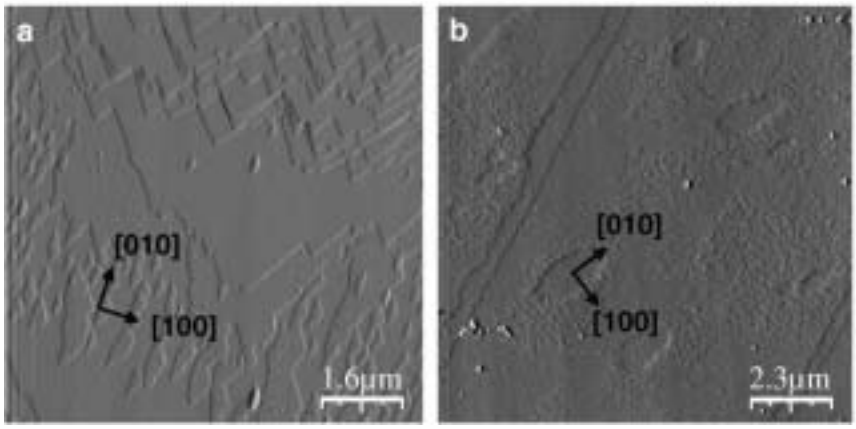

Fig. 1. AFM deflection images showing the dissolution of the celestite (001) face. (a) In deionised water. Both the retreating of cleavage steps and the formation of the etch pits with triangular shape can be observed. The steps edges defining the shape of the etch pits are parallel to the [010] and ⟨120⟩ directions. The orientation of etch pits alternate in successive monolayers. (b) In a 0.001 mol/l Na_2CO_3 aqueous solution. The etch pits become elliptical with long and short axis of the ellipse parallel to the [010] and [100] directions, respectively. Note the high surface roughness around the etch pits.

to the ⟨120⟩ and to the [010] directions (Fig. 1a). However, the shape of the etch pits changes when the surface is in contact with CO_3^{2-}-bearing aqueous solutions. Progressively, straight edges disappear and the etch pits become elliptical, with short and long axes parallel to the [100] and [010] directions, respectively. Fig. 1b shows the typical shape of the etch pits when the celestite (001) surface is in contact with a CO_3^{2-}-bearing aqueous solution.

Another interesting phenomenon observed is the alteration of the celestite (001) surface, which occurs simultaneously, or probably preceding, to the dissolution. This alteration is clearly shown by an increase in the roughness of the surfaces. This can be observed by comparing the aspect of the dissolving layer with the surface of the layer underneath, seen through the etch pits recently formed and on the area left uncovered by the steps retreating (Fig. 1b).

Some minutes after starting the alteration–dissolution process, the nucleation of a new phase on the celestite (001) surface is observed (Fig. 2d). The time elapsed between the injection of the CO_3^{2-}-bearing aqueous solution in the AFM fluid cell and the formation of the first nuclei (hereafter islands) decreases with the initial concentration of CO_3^{2-} in the aqueous solutions (e.g. 15 min for a solution $[Na_2CO_3] = 0.005$ mol/l and 45 min for a solution $[Na_2CO_3] = 0.001$ mol/l). Islands of the new phase form mainly on celestite cleavage steps and they grow more rapidly parallel to the celestite [010] direction rather than parallel to the [100] direction. With time, the coalescence of the islands leads to the complete covering of the original surface by a homogeneous layer after a period of time that decreases with the initial concentration of CO_3^{2-} in the aqueous solution (about 30 min for a solution $[Na_2CO_3] = 0.005$ mol/l and more than an hour for a solution $[Na_2CO_3] = 0.001$ mol/l). Fig. 2 shows a complete sequence of AFM images, where both the substrate dissolution and the formation of a layer by coalescence of islands can be observed. AFM measurements show that the height of the new layer is 2.75 ± 0.25 nm (Fig. 3).

Although the coalescence of islands progressively armours the substrate from further interaction with the aqueous solution, growth continues to progress during a period of time at a reduced rate, until it finally stops. While the islands grow at a reduced rate, the spreading of monolayers on top of them is clearly observed (Fig. 2f). The height of such a new layer is 2.9 ± 0.2 Å (Fig. 4).

3.2. *Kinetics of the interaction between celestite (001) surfaces and carbonate-bearing aqueous solutions*

The dissolution rate of the celestite (001) surface in contact with a CO_3^{2-}-bearing aqueous solution is higher than in pure deionised water. Moreover, an increase in CO_3^{2-} concentration results in an increase of the dissolution rate. In order to evaluate the dependence of the dissolution rates on the initial concentration of CO_3^{2-}, the changes in shape of the etch pits with time have been measured. As the typical shape of the etch pits when aqueous solutions contain CO_3^{2-} is elliptical and elongated along the [100] direction, the etch pits growth was followed by measuring the variation of their length parallel to the [100] and [010] directions. Fig. 5 shows the experimental data of the etch pits growth rate along the [100] and [010] directions versus the concentration of Na_2CO_3 in the aqueous solution in the range from 0.001 mol/l to 0.005 mol/l. The stronger dependence of the retreating velocity along the [010] direction upon carbonate concentration is consistent with the observed increasing elongation of the etch pits along that direction.

Once islands of the new phase form on the celestite (001) surface, the dissolution kinetics is strongly modified. Fig. 6 shows the opening of the etch pits along the [100] and [010] directions versus time when a 0.001 mol/l Na_2CO_3 aqueous solution is used. In this figure, open symbols represent the progressive increase of the size of one monolayer etch pits (3.4 Å in depth) formed in the absence of islands. Black symbols represent

Moreover, several authors have stated that the lack of intermediate compositions in natural occurring members of the $Ba_xSr_{1-x}CO_3$ solid solution cannot be the result of an unavailability of Ba or Sr in the growth medium [9,10]. Nevertheless, thermodynamic experimental studies have concluded that this solid solution is ideal and, consequently, complete [11,12]. This result, together with evidence of the replacement of barium–strontium sulphates by carbonates in nature, suggests that the compositional bimodality shown by $Ba_xSr_{1-x}CO_3$ solid solution could be inherited from precursor sulphates [7,8].

Mineral replacement reactions are common in the Earth's Crust. Under low temperature and pressure conditions, these reactions are frequently controlled by the coupling between the dissolution of a parent phase and the crystallization of a new one [13]. Furthermore, during mineral replacement, different textural characteristics of the original phase are preserved and it cannot be discarded that the same occurs with chemical information. In spite of the obvious importance of this type of processes, very few experimental works have addressed this problem. Consequently, both their kinetics and the mechanisms that govern the development of replacement processes remain obscure. In the knowledge of the authors, the only experimental work on the transformation involving barium–strontium sulphates and carbonates was carried-out by Suarez-Orduña et al. [14]. These authors studied the conversion of mineral celestite into strontianite under alkaline hydrothermal conditions. They concluded that celestite crystals in contact with carbonate-bearing solutions in the range of temperatures from 150 to 250 °C partially or totally transform into strontianite after reaction periods that varied between 1 and 96 h.

Since mineral replacement resulting from dissolution–crystallization coupling is a surface process, it is of interest to investigate the nanoscale interaction between potential replacing aqueous solutions and mineral surfaces. In this work, we present an in situ AFM experimental study of the molecular mechanisms involved in the interaction between celestite and Na_2CO_3 aqueous solutions at room temperature. This study is completed with SEM observations and EDX analysis of celestite (001) surfaces after the reaction with carbonate aqueous solutions. The results of this AFM–SEM combined study provide an insight into the celestite–strontianite replacement mechanisms.

2. Experimental procedure

2.1. AFM experiments

Experiments were carried-out at room temperature in an AFM equipped with a fluid cell (Digital Instruments Multimode) and working in contact mode. All the images shown in this work were taken in constant force mode while displaying both cantilever height and deflection signals. Silicon nitride tips (Veeco NP-S10) with a nominal force constant of $k = 0.06$–0.58 N/m were used. Optically clear celestite crystals were freshly cleaved parallel to (001) surface prior to each experiment. Then, aqueous solutions with different Na_2CO_3 concentrations and CO_3^{2-} activities were placed in contact with the celestite substrate (see Table 1). In all the experiments, the solution in contact with the celestite (001) surface was kept static in the AFM fluid cell. In this way, the aqueous solution composition changed as crystal dissolution and/or growth proceeded, i.e. the system evolved towards equilibrium. The process was monitored by taking images at intervals of 50–60 s. When neither the dissolution of the substrate nor the growth of the new phase were observed for long observation periods (more than 30 min), the experiments were considered to be over.

Table 1
Na_2CO_3 concentrations and CO_3^{2-} activities (calculated using PHREEQc) of the aqueous solutions used in the experiments

Experiment number	Na_2CO_3 concentration (mol/l)	$a(CO_3^{2-})$
1	0.001	5.079×10^{-4}
2	0.002	1.043×10^{-3}
3	0.003	1.534×10^{-3}
4	0.004	1.984×10^{-3}
5	0.005	2.402×10^{-3}
6	0.05	1.138×10^{-2}
7	0.1	1.600×10^{-2}

Height images were used to measure the thickness of the layers formed on the celestite (001) surface. Systematic measurements of the dissolution rate of the celestite (001) surface along the [100] and [010] directions of the etch pits were taken on deflection AFM images corresponding to different runs of the same experiments (Fig. 1a). Each run was repeated 2–3 times in order to minimize random errors.

2.2. SEM observations and EDX analysis

Once the experiments were over, celestite crystals were removed from the fluid cell of the AFM, rapidly dried by blowing pressurised air on their surfaces and observed by SEM (JEOL JSM 6400). The composition of the newly-formed phase grown on the celestite (001) surfaces was analyzed using a Link-analytical EDX.

3. In situ AFM observations

3.1. Evolution of the nanotopography of celestite (001) faces

Immediately after placing the celestite (001) surface in contact with a CO_3^{2-}-bearing aqueous solution, the dissolution is observed. The dissolution of the surface occurs by both the retreating of monolayer cleavage steps and by the nucleation and growth of the etch pits by half a unit cell in depth (3.4 Å). Typically, when a freshly cleaved celestite (001) face is placed in contact with deionised water, etch pits show a shape defined by monolayer step edges parallel

[6] M. Prieto, A. Putnis, L. Fernández-Díaz, Geol. Mag. 130 (1993) 289.
[7] M. Prieto, A. Fernández-González, L. Fernández-Díaz, Geochim. Cosmochim. Acta 61 (1997) 3383.
[8] A. Baldasari, J.A. Speer, Am. Miner. 64 (1979) 742.
[9] L.L.Y. Chang, W.R. Brice, Am. Miner. 57 (1972) 155.
[10] J.A. Speer, M.L. Henseley-Dunn, Am. Miner. 61 (1976) 1001.
[11] L.L.Y. Chang, J. Geol. 73 (1965) 346.
[12] L.L.Y. Chang, Am. Miner. 57 (1971) 1660.
[13] A. Putnis, Min. Mag. 66 (2002) 689.
[14] R. Suárez-Orduña, J.C. Rendón-Angeles, J. López-Cuevas, K. Yanagisawa, J. Phy.: Condens. Matter 16 (2004) 1331.
[15] H. Shindo, K. Shitagami, S. Kondo, A. Seo, J. Cryst. Growth 198 (1999) 253.
[16] P. Risthaus, D. Bosbach, U. Becker, A. Putnis, Colloids Surf., A Physicochem. Eng. Aspects 191 (2001) 201.
[17] A.S. Lea, T.T. Hurt, A. El-Azab, J.E. Amonette, D.R. Baer, Surf. Sci. 524 (2003) 63.
[18] C. Pérez-Garrido, L. Fernández-Díaz, C.M. Pina, M. Prieto, Macla 6 (2006) 355.
[19] C.M. Pina, N. Sánchez-Pastor, L. Fernández-Díaz, C. Pérez-Garrido, M. Prieto, Geochim. Cosmochim. Acta 70 (18) (2006) A494.
[20] W.M.M. Heijnen, Neues Jahrbuch Mineral Abh. 154 (1986) 223.
[21] L.L.Y. Chang, R.A. Howie, J. Zussman, Non-silicates: Sulphates, Carbonates, Phosphates, Halides, Rock-Forming Minerals, vol. 5B, The Geological Society, 1998.
[22] M.A. Simonov, S.I. Troyanov, Vestn. Mosk. Uni. 4 (1987) 77.
[23] A.A. Chernov, Modern Crystallography III (Crystal Growth), Springer-Verlag, 1984.
[24] M. Prieto, A. Putnis, L. Fernández-Díaz, Geol. Mag. 127 (1990) 485.
[25] M. Prieto, L. Fernández-Díaz, S. López-Andrés, J. Cryst. Growth 108 (1994) 770.
[26] H.C. Helgeson, Geochim. Cosmochim. Acta 32 (1968) 853.
[27] M. Prieto, P. Cubillas, A. Fernández-González, Geochim. Cosmochim. Acta 67 (2003) 3859.
[28] C.M. Pina, L. Fernández-Díaz, M. Prieto, A. Putnis, Geochim. Cosmochim. Acta 64 (2000) 215.